

Article

Effect of Cu₂O Sputtering Power Variation on the Characteristics of Radio Frequency Sputtered p-Type Delafossite CuCrO₂ Thin Films

Sreeram Sundaresh , Akash Hari Bharath  and Kalpathy B. Sundaram

Department of Electrical and Computer Engineering, University of Central Florida, Orlando, FL 32826, USA

* Correspondence: sreeram.sundaresh@knights.ucf.edu

Abstract: For the first time, the effect of Cuprous Oxide (Cu₂O) sputtering power variation on the radio frequency sputtered Copper Chromium Oxide (CuCrO₂) thin films was studied. In this work, the sputtering power of Cr₂O₃ was held constant at 200 W while the sputtering power of the Cu₂O target was varied from 10 to 100 W. The films were subsequently annealed at 650 °C in N₂ ambiance. The effects of Cu₂O sputtering power variation on the structural, optical, and electrical properties of the films have been reported in this work. X-ray diffractometer (XRD) study revealed that the single-phase delafossite structure of CuCrO₂ was only obtained at Cu₂O sputtering power of 50 W. X-ray photoelectron spectroscopy (XPS) analysis further established the results of XRD study where Cu in 1+ oxidation state was identified in thin films obtained at 50 W of Cu₂O sputtering power. The optical studies were conducted in this work on all the post-deposition annealed films in the wavelength range of 200–800 nm. The energy dispersive x-ray spectroscopy (EDS) study revealed a near stoichiometric composition ratio of 1:1.06 of Cu:Cr at% obtained in the films sputtered with 50 W of Cu₂O sputtering power. The highest optical transmission of ~81% and the highest optical bandgap of 3.21 eV were observed for single-phase CuCrO₂ thin films. The optical transmission and the optical bandgap were found to decrease with an increase in the Cu₂O sputtering power. The electrical study performed on all the post-deposition annealed films revealed that the lowest resistivity of 0.652 Ω-cm was identified for single-phase CuCrO₂ thin films obtained at 50 W of Cu₂O sputtering power.



Citation: Sundaresh, S.; Bharath, A.H.; Sundaram, K.B. Effect of Cu₂O Sputtering Power Variation on the Characteristics of Radio Frequency Sputtered p-Type Delafossite CuCrO₂ Thin Films. *Coatings* **2023**, *13*, 395. <https://doi.org/10.3390/coatings13020395>

Academic Editor: Zhongkai Cheng

Received: 31 December 2022

Revised: 1 February 2023

Accepted: 7 February 2023

Published: 9 February 2023



Copyright: © 2023 by the authors. Licensee MDPI, Basel, Switzerland. This article is an open access article distributed under the terms and conditions of the Creative Commons Attribution (CC BY) license (<https://creativecommons.org/licenses/by/4.0/>).

Keywords: delafossite CuCrO₂; RF sputtered CuCrO₂; Cu₂O power variation; p-type CuCrO₂; CuCrO₂ thin films; CuCrO₂ transmission; CuCrO₂ bandgap; CuCrO₂ resistivity; CuCrO₂ XRD; CuCrO₂ XPS; CuCrO₂ EDS

1. Introduction

Transparent Conducting Oxides (TCOs) are a unique class of compounds that combine the properties of being optically transparent and electrically conductive at the same time [1]. Due to this, TCOs have attracted significant attention in recent years and find applications in transparent optoelectronic devices, light-emitting diodes, solar cells, and thin film transistors [2–4]. For the aforementioned applications, it is imperative to have p-type and n-type semiconducting layers. There has previously been a large number of research studies that have been carried out on discovering materials depicting n-type semiconducting characteristics at room temperature. Some of them include In₂O₃ [5–7], Sn-doped In₂O₃ (ITO) [8–10], Sc-doped ZnO [11,12], SnO₂ [13,14], Al-doped ZnO (AZO) [15–17], and CdSnO₂ [18,19]. However, there has been a lack of research work on p-type TCOs, which is severely restricting the development of transparent pn-junction-based devices in transparent electronics applications [20,21]. This is because p-type TCOs have previously been shown to possess either good optical transparency (>80%) or low electrical resistivity (<10^{−2} Ω-cm) [1,2]. P-type TCOs with both the aforementioned properties have been difficult to develop.

The reason for this behavior of p-type TCOs can be attributed to the position of the valence band level of the metal oxides. The valence band level of metal oxides is

far lower lying than its metal counterpart. Due to this, sufficiently higher energy is required for the mobilization of holes through the crystal lattice [3]. One solution to solve this problem is to perform doping [22]. However, the electronegativity of oxygen has been previously reported to be very high at 3.44. The only element to have higher electronegativity is fluorine at 3.98 [23,24]. Due to this, the holes are strongly attracted to the O₂ ions, further restricting their movement across the lattice. This is the prime reason for the decreased electrical conductivity observed in p-type TCOs as compared to their n-type counterpart [25,26].

Hosono et al. proposed the concept of Chemical Modulation of Valence Band (CMVB) to alleviate this issue [27]. They found that due to the addition of appropriate cations such as Cu⁺, the added cation forms a strong covalent bond with the oxygen ions since the energy difference between Cu 3d¹⁰ and O 2p⁶ is very small. During this process, the energy level of O-2p is raised and the coulombic force of attraction between oxygen ions and holes is reduced. This reduces the barrier height which ultimately leads to a lower energy requirement for holes to cross the barrier. The optical transparency of the films is preserved during this process since the closed shell nature of Cu 3d¹⁰ prevents the coloration of the deposited films [25].

The appropriate cation for this process could include Cu⁺ or Ag⁺. However, previous works in the literature have reported that the electrical resistivity of the films obtained using Ag⁺ cation is very high, of the order of 10⁴ to 10⁶ Ω-cm [28]. The films obtained with the addition of Cu⁺ cation using this technique are called Cu-based delafossites. Reports indicate that Cu-based delafossites typically exhibit high optical transparency (60%–85%) along with low electrical resistivity (5 × 10^{−2} to 8 × 10^{−3} Ω-cm) [26,29]. Similar results have been obtained by Saikumar et al. where a dual sputtering approach for CuGaO₂ synthesis was employed [20]. The general form of Cu-based delafossites is CuMO₂, where Cu is the positive monovalent cation (Cu⁺), M = Al³⁺, Cr³⁺, In³⁺, Ga³⁺, Sc³⁺, and Y³⁺ (trivalent cation), and oxygen is the divalent anion (O^{2−}) [30]. Among all the Cu-based delafossites, CuCrO₂ is a promising material since it shows a valuable trade-off between optical transparency and electrical conductivity [26,29]. CuCrO₂ has previously been synthesized at a low temperature, has good thermal stability in the air, and has room temperature resistivity of 0.66 Ω-cm with an optical transmission of ~60% [26,31,32].

This research work involves the deposition of the delafossite structure of CuCrO₂ thin films using the dual-target RF magnetron sputtering technique of Cu₂O and Cr₂O₃ targets. Further, the effect of variation of Cu₂O sputtering power from 10 W to 100 W on the electrical, optical, and structural properties of the films has been investigated for the first time. The Cr₂O₃ sputtering power was maintained at 200 W. The deposited films underwent post-deposition annealing at 650 °C in N₂ ambiance. Single-phase delafossite structures of p-CuCrO₂ exhibiting superior electrical and optical properties were obtained in this work.

2. Experimental Section

2.1. Deposition of CuCrO₂ Thin Films

The dual target radio frequency (RF) magnetron sputtering technique of the 3" diameter Cu₂O target (99.99% purity, Maideli Advanced Materials Co., Ltd., Jiangyin, China) and 3" diameter Cr₂O₃ target (99.99% purity, Maideli Advanced Materials Co., Ltd., Jiangyin, China) was employed for the deposition of 125 nm thick CuCrO₂ thin films in this work. The deposition of the films analyzed in this research was carried out using AJA international ultra-high vacuum three-gun sputtering equipment. All the film depositions were carried out on fused quartz substrates. The substrates were cleaned thoroughly using acetone, methanol, and DI water, and blow-dried with nitrogen gas before film depositions. Two separate RF sources (13.6 MHz) were used to control the sputtering power of the two targets used in this research. Ultra-high purity Ar gas at a flow rate of 10 sccm was used as the sputtering gas. The sputtering power of Cr₂O₃ was held constant at 200 W while the sputtering power of the Cu₂O sputtering target was varied between 10 and 100 W.

The films obtained with 100 W of Cu₂O sputtering power appeared dark after annealing, subsequently leading to very low transmission. Since the motive behind this research is to obtain transparent yet conductive thin films, the final sputtering power of 100 W was chosen for the Cu₂O target. All the film depositions were carried out only after the chamber pressure reached 5×10^{-7} Torr. Uniform film thickness was ensured by rotating the substrate holder at a constant speed of 20 rpm during deposition. The substrate temperature was held constant at 400 °C (sputtering tool limit) during all the film depositions. The films were post-deposition annealed at 650 °C in N₂ (grade: Ultra-High purity) ambience in a tube furnace for 4 h. During the annealing process, the N₂ flow rate was held constant at 300 sccm. The annealing temperature was decided based on the previous literature which suggested that the delafossite structure of p-type CuCrO₂ thin films can be obtained at a much lower annealing temperature of ~600 °C [33–38]. The deposition parameters maintained during this research work are listed in Table 1.

Table 1. Deposition parameters maintained during deposition of CuCrO₂ thin films.

Deposition Parameter	Specification
Sputtering gases	Ar
Base pressure	5×10^{-7} Torr
Deposition pressure	10 mTorr
RF power (Cr ₂ O ₃)	200 W
RF power (Cu ₂ O)	10 W, 30 W, 50 W, 75 W, 100 W
Substrate temperature	400 °C
Sputtering gas flow rate	10 sccm
Thickness of deposited film	125 nm
Annealing temperatures	650 °C
Annealing gas and flow rate	N ₂ at 300 sccm

2.2. Film Characterization

The deposited film thickness was verified using Veeco Dektak 150 Surface Profiler. To identify the materials based on the diffraction patterns, XRD analysis was carried out using the PANalytical Empyrean XRD system (Malvern Panalytical, Westborough, MA, USA), from a Cu radiation source at 45 kV and 40 mA. The diffraction pattern recorded at 2θ angles from 25° to 70° was analyzed using HighScore Plus Software (Malvern Panalytical, Westborough, MA, USA). The elemental composition of the films and their oxidation states were analyzed using ESCALAB 250 Xi + X-ray photoelectron spectroscopy (XPS) (ThermoFisher Scientific, Waltham, MA, USA) with monochromatic Al K α source (1486.7 eV). An in-built EX06 ion source was used to perform ion beam milling of the film surface to remove the surface oxides before XPS analysis. Further, XPS data were analyzed using Thermo Fischer Scientific Avantage software (v5.9902) to perform elemental composition analyses, functional group analyses, and XPS peak fitting. The optical transmission of the films was measured using the Cary 100 UV-Visible Spectrophotometer (Varian Analytical Instruments, Walnut Creek, CA, USA) at light wavelengths between 200 and 800 nm. Optical bandgap studies of the films were conducted using the Tauc plot method on the absorption data. The conductivity type of the post-deposition annealed films was checked using the hot probe method and four-point probe (Magn-tron Instruments Model M-700). The resistivity of the post-deposition annealed films was measured by patterning parallel aluminum (Al) contact pads as shown in Figure 1. To pattern the Al contact pad windows, a photolithography process was adopted, which was followed by Al metal deposition using a thermal evaporation process, and removal of photoresist using a lift-off technique. Using IV characteristics obtained from the Keithley 2450 source meter unit, the resistance (R) of the thin films was calculated. The resistivity (ρ) of the thin films was identified using Equation (1).

$$\rho = R * \frac{A}{L} \quad (1)$$

where 'R' is the resistance, 'L' is the length, and 'A' is the area of the cross-section.

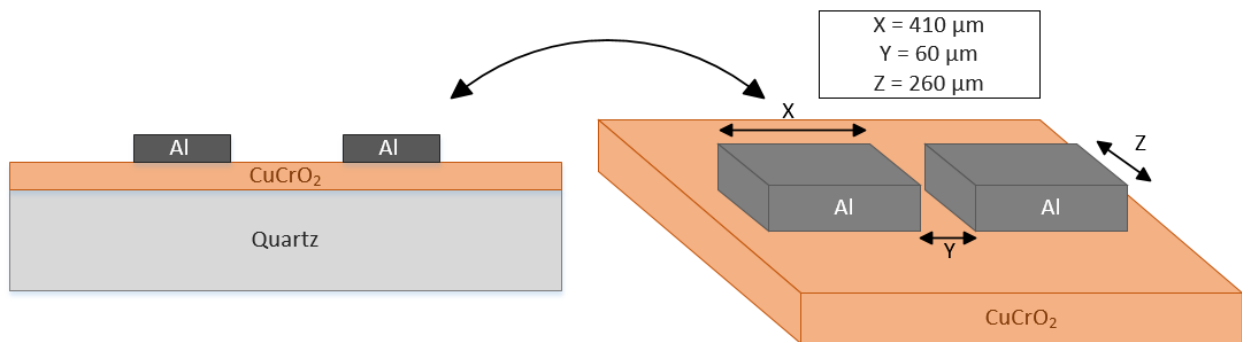
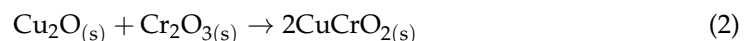


Figure 1. Two-dimensional and three-dimensional representation of Al pads deposited on CuCrO₂ thin film used for electrical measurements.

3. Results and Discussion

3.1. XRD Analysis

The XRD diffractograms of the films obtained at various sputtering powers of Cu₂O annealed at 650 °C are shown in Figure 2. The 2θ limits in Figure 2 have been adjusted to omit the amorphous peak of quartz that appeared in all the films between 18 and 25°. Nanocrystalline growth was observed in all the films as clear diffraction peaks were observed. The crystallization directions of all the diffraction peaks identified from the XRD analysis of all the samples have been marked in Figure 2. It can be observed from Figure 2a that at low Cu₂O sputtering power of 10 W, only peaks pertaining to Cr₂O₃ and CuCr₂O₄ were observed. As seen in Figure 2b, with a further increase in the sputtering power to 30 W, the peak intensity of Cr₂O₃ was reduced, and additional peaks belonging to the CuCr₂O₄ phase started emerging. By looking at the intensity of the peaks obtained in the XRD diffractograms of the films shown in Figure 2a,b, we can comparatively say that the films obtained with 10 W of Cu₂O sputtering power are Cr₂O₃ richer as compared to the films obtained with 30 W of Cu₂O sputtering power. The aforementioned dual phase nature of films disappeared as the sputtering power was increased to 50 W. Single phase delafossite structure of CuCrO₂ was obtained at 50 W of Cu₂O sputtering power, which can be confirmed from Figure 2c. The diffraction peaks identified as CuCrO₂ in this film indexed well to delafossite CuCrO₂ (ICDD: 98-016-3253) structure. The major diffraction peaks identified at 2θ angles of 31.343°, 35.186°, 36.377°, 40.845°, 55.812°, 62.353°, and 65.419° were indexed to (006), (101), (012), (104), (018), (110), and (1010) of CuCrO₂, respectively. The delafossite structure of CuCrO₂ is comprised of two structural polytype space groups, 2H-R3m and 3R-P63/mmc. The diffraction pattern obtained in this research work for 50 W of Cu₂O sputtering power indexed well to 2H-R3m space group. Similar diffraction peaks corresponding to the delafossite structure of CuCrO₂ were obtained by Ahmadi et al. [39]. The additive reaction that governs the formation of CuCrO₂ is shown in Equation (2) [40,41].



From Figure 2d,e, it can be noticed that as the Cu₂O sputtering power is increased further to 75 W and 100 W, the single-phase nature of the films gets transformed into two-phase structures. This is accompanied by the appearance of the CuO phase along with the presence of the CuCrO₂ phase. At 75 W of Cu₂O sputtering power, the smaller intensity peaks corresponding to the CuCrO₂ delafossite phase observed in Figure 2c completely disappear, leaving only two high intensity CuCrO₂ peaks seen in Figure 2d. On comparing Figure 2d,e, stronger peaks corresponding to the CuO phase were observed at 100 W of Cu₂O sputtering power as compared to results obtained for 75 W. This indicated that as the Cu₂O sputtering power was increased from 10 to 100 W, there is a gradual shift from the films being Cr₂O₃ rich to eventually being CuO phase rich. Hence, it is safe to conclude

that at the Cu_2O sputtering power of 50 W, a single-phase delafossite structure of CuCrO_2 thin films was obtained and no peaks of CuO , Cr_2O_3 , or CuCr_2O_4 were observed. Table 2 shows the relationship between the Cu_2O sputtering powers and the phases identified at each of them.

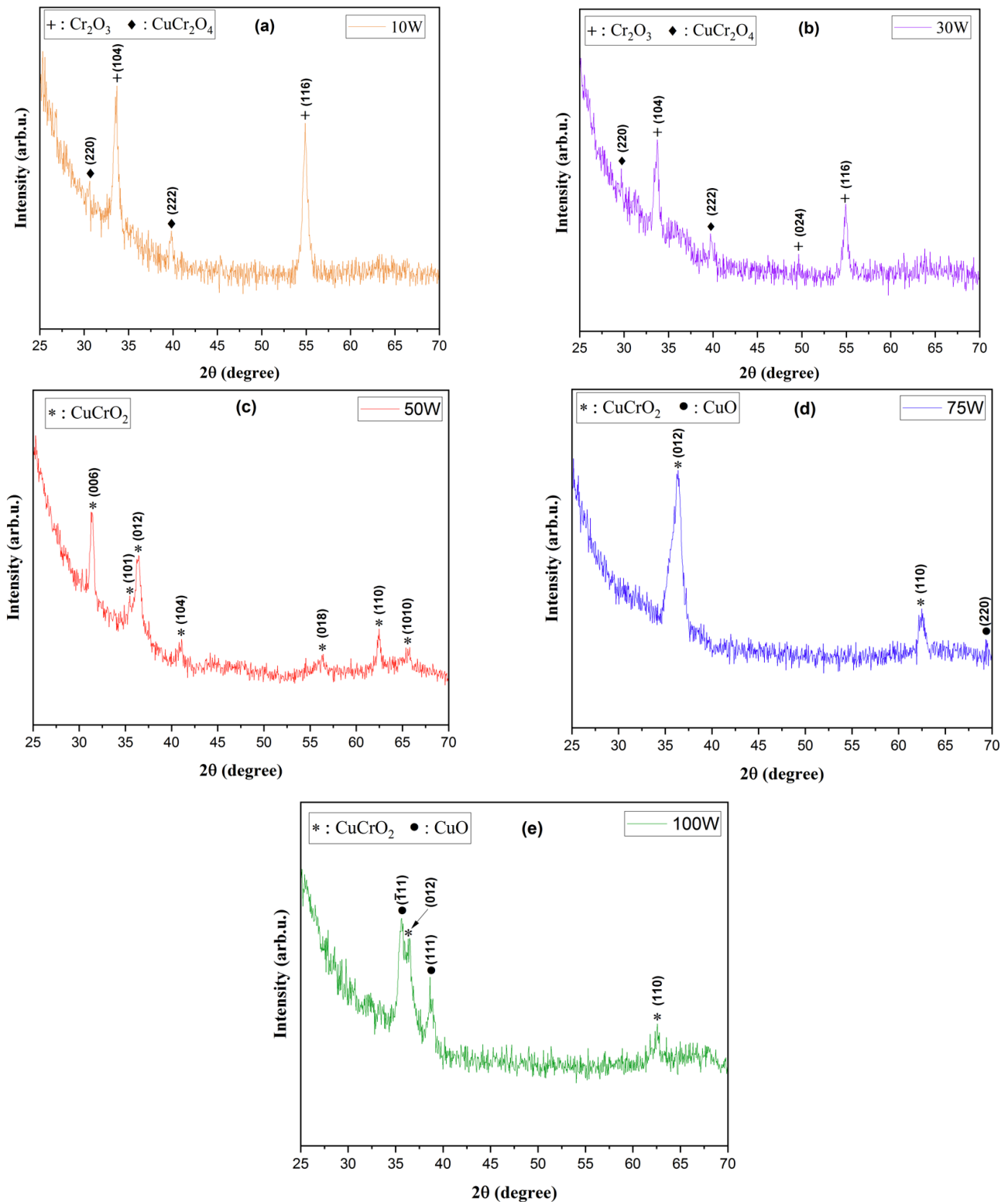


Figure 2. XRD diffractograms of the films obtained after post-deposition annealing at 650°C at Cu_2O sputtering powers of (a) 10 W, (b) 30 W, (c) 50 W, (d) 75 W, and (e) 100 W.

Table 2. Phases identified through XRD analysis in the films sputtered with different Cu₂O sputtering power.

Cu ₂ O Sputtering Power (W)	Phases Identified
10	Cr ₂ O ₃ + CuCr ₂ O ₄
30	Cr ₂ O ₃ + CuCr ₂ O ₄
50	CuCrO ₂ (delafossite)
75	CuCrO ₂ + CuO
100	CuCrO ₂ + CuO

3.2. XPS Analysis

The XPS survey spectra of CuCrO₂ thin films are shown in Figure 3a. From the survey spectrum, it can be confirmed that only peaks pertaining to Cu, Cr, and O were identified. The individual Cu-2p, Cr-2p, and O-1s core level spectra for the different Cu₂O sputtering powers have been resolved and are shown in Figure 3b–f. It is important to note that copper in copper chromium oxide thin films mainly exists in two oxidation states of 1+ and 2+. Previous research has shown that the oxidation state of copper is 1+ for the CuCrO₂ (delafossite structure) phase and it exists in the 2+ oxidation state for CuCr₂O₄ (spinal structure) phase [40–43]. The Cu¹⁺ species can be distinguished from the Cu²⁺ species through the identification of satellite peaks in the Cu-2p core level spectrum. In the Cu-2p core level spectrum, the Cu-doublet comprising Cu 2p_{1/2} and Cu 2p_{3/2} are classified as the main peaks of Cu. Apart from the main peaks, in the case of Cu²⁺ species, satellite peaks (shake-up satellite features) corresponding to the main peaks are observed at a higher energy level than the main peaks [44]. The absence of satellite peaks in the case of Cu¹⁺ species is its distinguishing feature [43,45–47]. The reason for this behavior has been previously attributed to the metal–ligand charge transfer that takes place during the photoemission process [48]. In addition to this, the presence of Cu¹⁺ species in the film can be confirmed by the presence of Cu Auger peak (Cu LMM) in the same range of energies of the Cr core level XPS spectrum. The Cu LMM peak would be absent for the films signifying the presence of Cu²⁺ species [41]. Using the core level spectrums, the oxidation states, binding energies, peak positions, satellite peak positions, Full-Width Half Maximum (FWHM), and the spin-orbit split energy between the main peaks of the elements are elucidated in Table 3. The description listed henceforth in this section would majorly encompass the key differences that were observed between the core level spectra of the films obtained by varying the Cu₂O sputtering power.

From Figure 3(bi), it can be observed that the Cu content in the films sputtered with 10 W of Cu₂O sputtering power was not enough to be detected through XPS analysis. This is contrary to the results obtained through XRD analysis, where CuCr₂O₄ phases were observed. A possible reason for this observation can be attributed to the fact that XPS is a surface analysis technique while XRD is a bulk analysis technique. Hence, XRD analysis was able to identify the CuCr₂O₄ phase present in the bulk of the film while XPS could not detect any Cu presence on the surface. The main peaks of Cu-2p doublet are Cu 2p_{3/2} and Cu 2p_{1/2} (marked by peaks 1 and 2 in Figure 3(bi–fi)). With the increase in the Cu₂O sputtering power to 30 W, Cu 2p_{3/2} and Cu 2p_{1/2} peaks started showing up clearly in the Cu-2p core level spectrum. However, weak but detectable satellite peaks corresponding to the Cu-2p doublet are also observed at a higher energy level compared to their main peaks. This observation can be seen in Figure 3(ci). This confirmed the presence of Cu²⁺ species in the film sputtered with 30 W of Cu₂O sputtering power. This further corroborates with our findings of XRD analysis where only the CuCr₂O₄ phase was observed in which Cu has been previously reported to be in a 2+ oxidation state [49,50]. In Figure 3(di), the satellite peaks completely disappear for the film obtained at 50 W of Cu₂O sputtering power. This is due to the identification of a single-phase CuCrO₂ delafossite structure through XRD analysis in this film. Similar disappearance of satellite peaks in single-phase CuCrO₂ thin films have been reported previously [51,52]. Hence Cu can be confirmed to be in a 1+ oxidation state in the film obtained with 50 W of Cu₂O sputtering power and the

successful formation of a single-phase CuCrO_2 delafossite structure in the film. Looking at Figure 3(ei,fi), it can be noticed that as the Cu_2O sputtering power is increased further to 75 W and 100 W, satellite peaks corresponding to the Cu-2p doublet start to emerge again and the single-phase structure of CuCrO_2 disintegrates. The reason for this can be attributed to the identification of CuO phases. This leads to the confirmation that Cu is present in a 2+ oxidation state as well in the films sputtered with 75 W and 100 W of Cu_2O sputtering power.

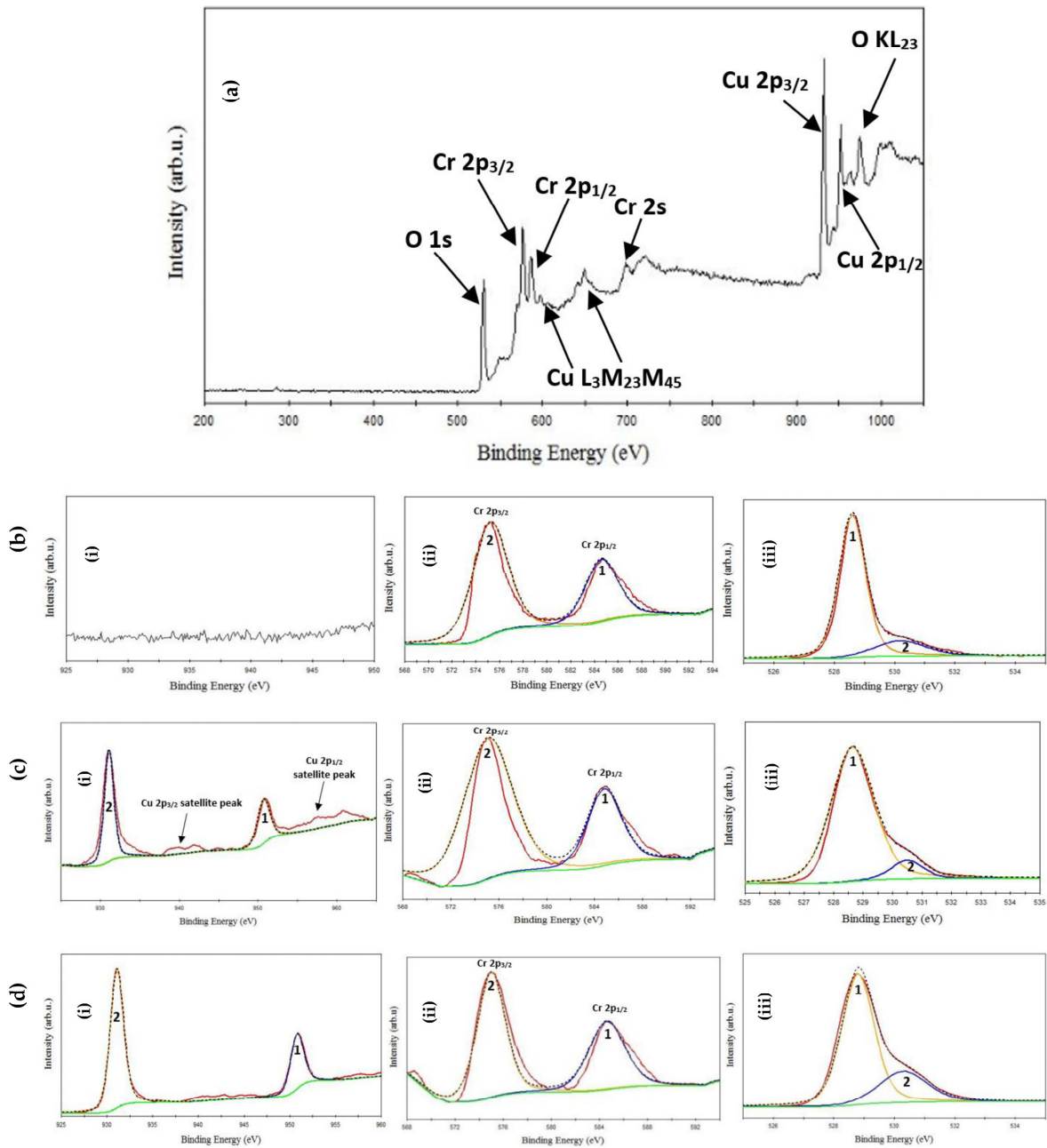


Figure 3. Cont.

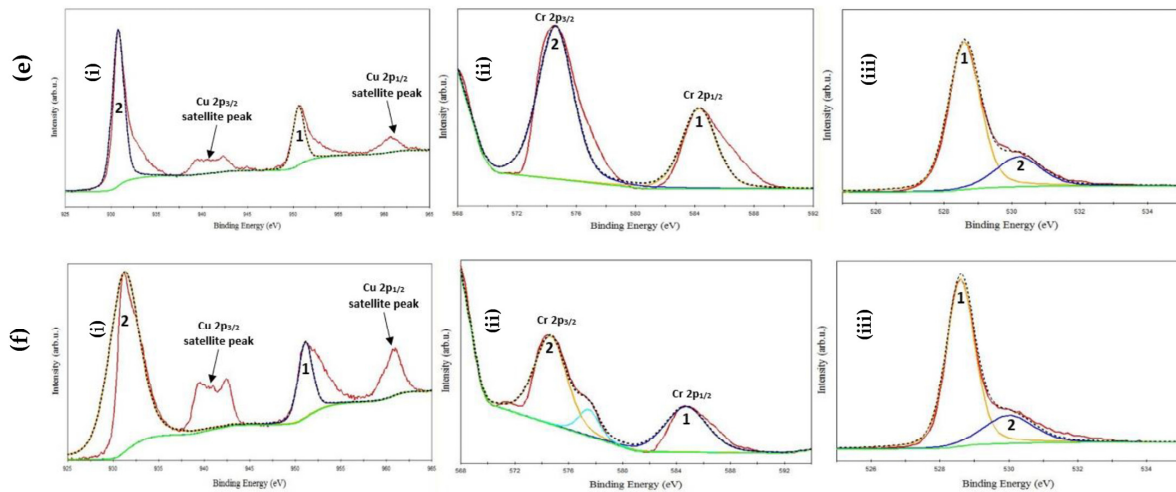


Figure 3. (a) XPS survey spectrum, (i) Cu-2p core level spectrum, (ii) Cr-2p core level spectrum, (iii) O-1s core level spectrum of thin films sputtered with (b) 10 W, (c) 30 W, (d) 50 W, (e) 75 W, (f) 100W of Cu₂O sputtering power.

Table 3. Full-Width Half Maximum (FWHM), peak positions, satellite peak positions, and their respective binding energy of the films under study.

Cu ₂ O Sputtering Power	Peak	Oxidation State	Binding Energy (eV)	Spin-Orbit Split Energy (eV)	Satellite Peak (eV)	FWHM (eV) of Main Peaks
10 W	Cu 2p _{3/2}	Cu ²⁺	-	-	-	-
	Cu 2p _{1/2}	Cu ²⁺	-	-	-	-
	Cr 2p _{3/2}	Cr ³⁺	576.37 eV	$\Delta_{Cr-2p} = 9.4$ eV	-	3.55 eV
	Cr 2p _{1/2}	Cr ³⁺	585.77 eV		-	3.31 eV
30 W	Cu 2p _{3/2}	Cu ²⁺	932.27 eV	$\Delta_{Cu-2p} = 19.6$ eV	941.81 eV 939.35 eV	1.88 eV
	Cu 2p _{1/2}	Cu ²⁺	951.87 eV		960.70 eV	1.42 eV
	Cr 2p _{3/2}	Cr ³⁺	576.27 eV	$\Delta_{Cr-2p} = 9.7$ eV	-	4.80 eV
	Cr 2p _{1/2}	Cr ³⁺	585.97 eV		-	3.41 eV
50 W	Cu 2p _{3/2}	Cu ¹⁺	932.27 eV	$\Delta_{Cu-2p} = 19.7$ eV	-	1.76 eV
	Cu 2p _{1/2}	Cu ¹⁺	951.97 eV		-	1.68 eV
	Cr 2p _{3/2}	Cr ³⁺	576.17 eV	$\Delta_{Cr-2p} = 9.6$ eV	-	2.74 eV
	Cr 2p _{1/2}	Cr ³⁺	585.77 eV		-	3.57 eV
	Cu LMM	Cu ¹⁺	569.92 eV	-	-	1.82 eV
75 W	Cu 2p _{3/2}	Cu ²⁺	931.97 eV	$\Delta_{Cu-2p} = 19.6$ eV	939.51 eV 942.32 eV	1.57 eV
	Cu 2p _{1/2}	Cu ²⁺	951.77 eV		960.72 eV	1.50 eV
	Cr 2p _{3/2}	Cr ³⁺	575.77 eV	$\Delta_{Cr-2p} = 9.7$ eV	-	2.80 eV
	Cr 2p _{1/2}	Cr ³⁺	585.47 eV		-	2.73 eV
		Cu LMM	Cu ¹⁺	568.07 eV	-	-
100 W	Cu 2p _{3/2}	Cu ²⁺	932.39 eV	$\Delta_{Cu-2p} = 19.88$ eV	939.50 eV 942.40 eV	3.93 eV
	Cu 2p _{1/2}	Cu ²⁺	952.27 eV		961.00 eV	1.88 eV
	Cr 2p _{3/2}	Cr ³⁺	575.83 eV	$\Delta_{Cr-2p} = 10.04$ eV	-	2.85 eV
	Cr 2p _{1/2}	Cr ³⁺	585.87 eV		-	1.86 eV
		Cu LMM	Cu ¹⁺	568.05 eV	-	-

Analysis of the Cr-2p core level spectrum of the films obtained at varying Cu₂O sputtering power was conducted using the results shown in Figure 3(bii–fii). All the films analyzed in this study showed Cr-2p doublet (Cr 2p_{1/2} and Cr 2p_{3/2}) (marked by peaks 1 and 2 in Figure 3(bii–fii)) at the binding energies listed in Table 3. Looking at Figure 3(bii) and Figure 3(cii), an important observation can be made in the Cr-2p spectrums of the films. At lower Cu₂O sputtering powers of 10 W and 30 W, no Cu LMM peak was observed. As mentioned before, the presence of Cu LMM peak signifies the presence of Cu 1+ species in the film. This leads to the deduction that no Cu 1+ species are present in the films sputtered with 10 W and 30 W of Cu₂O. Our XRD results were in agreement with the results stated previously, which indicated the presence of only the CuCr₂O₄ phase. With the increase in the Cu₂O sputtering power above 30 W, it can be noticed that the Cu LMM peak started showing up in the Cr-2p core level spectrums of the respective films shown in Figure 3(dii–fii). This observation signified the presence of Cu 1+ species in these films, which corroborated with the XRD results of these films that identified the presence of CuCrO₂ phase in the film at Cu₂O sputtering powers above 30 W. In addition to the main peaks of Cr-2p discussed above, only the film sputtered with Cu₂O sputtering power of 100 W shows an additional peak at 578.67 eV which corresponds to Cr (III) oxide [53,54]. However, it is important to note that only the film sputtered with 50 W of Cu₂O sputtering power showed the presence of Cu in the 1+ oxidation state. Moreover, from XPS analysis, it can be safely said that Cr exists in a 3+ oxidation state in all the analyzed films. This leads to the interpretation of the presence of a single-phase delafossite structure of CuCrO₂ in the film sputtered with 50 W of Cu₂O sputtering power.

The core level spectrum of O-1s obtained at different Cu₂O sputtering power is shown in Figure 3(biii–fiii). All the films analyzed showed two peaks that have been resolved. The peak at the lower energy level can be attributed to the lattice oxygen while the peak at the higher energy level can be attributed to the chemisorbed oxygen in the films (marked by peaks 1 and 2 in Figure 3(biii–fiii)) [41,55,56]. It is safe to conclude with the help of XRD analysis and XPS results that a single-phase CuCrO₂ delafossite structure can be synthesized at a Cu₂O sputtering power of 50 W.

A comparison between the FWHM of the O-1s peaks of the films studied in this research is shown in Figure 4, through which an important observation can be made. It can be seen that for the film sputtered with 10 W of Cu₂O, the FWHM of O-1s spectra was obtained as 1.04 eV. The FWHM of the O-1s peak suddenly rises to 1.70 eV for the films sputtered with 30 W of Cu₂O. A possible explanation can be made by correlating the FWHM values with the XRD results obtained in this research. At 10 W of Cu₂O sputtering power, sharp and high intensity peaks of Cr₂O₃ were observed and very small intensity peaks of CuCr₂O₄ were identified. As the sputtering power was increased to 30 W, the intensity of Cr₂O₃ peaks decreased and more peaks relating to CuCr₂O₄ were observed. As a result of change in the number of chemical bonds, an initial increase in the FWHM of the O-1s peak was observed. The occurrence of phase-pure CuCrO₂ at 50 W of Cu₂O sputtering power caused the FWHM of O-1s to drop to 1.26 eV. It can be noticed from Figure 4 that with the occurrence of delafossite structure of CuCrO₂ in the films, the FWHM of O-1s peak started dropping from a peak value of 1.70 eV. With further increase in the Cu₂O sputtering power, highly intense and sharp peaks corresponding to CuCrO₂ were identified in the XRD diffractograms. These factors may have possibly led to further drop in the FWHM of O-1s peak as seen in Figure 4.

3.3. EDS Study

EDS incorporated in the FESEM tool was used to obtain the Cu:Cr at% ratio of all the samples studied in this research. The comparison between the Cu:Cr at% ratio of all the post-deposition annealed samples is listed in Table 4. At 10 W of Cu₂O sputtering power, the Cu:Cr ratio was obtained as 1:5.55. As the Cu₂O sputtering power was increased to 100 W, the Cu:Cr ratio changed to 1:0.35. As expected, with the increase in the Cu₂O sputtering power, higher content of Cu was identified in the film. The films transformed

from being Cr_2O_3 rich at 5 W of Cu_2O sputtering power to being Cu rich at 100 W of Cu_2O sputtering power. The single phase CuCrO_2 thin films obtained at 50 W of Cu_2O sputtering power exhibited a near stoichiometric Cu:Cr at% ratio of 1:1.06. This result correlated well with the XRD and XPS results where single-phase delafossite nature of CuCrO_2 was identified at 50 W of Cu_2O sputtering power.

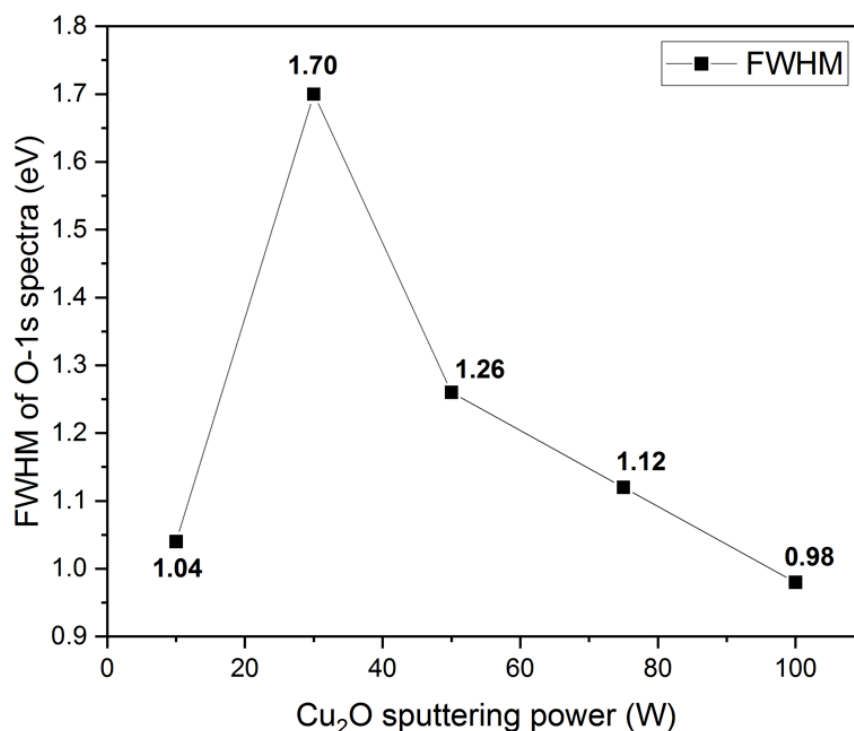


Figure 4. Variation of FWHM of O-1s core level spectra with varying Cu_2O sputtering powers.

Table 4. Cu:Cr at% ratio comparison of films obtained with different Cu_2O sputtering powers.

Cu_2O Sputtering Powers (W)	Cu:Cr at% Ratio
10	1:5.55
30	1:2.40
50	1:1.06
75	1:0.64
100	1:0.35

3.4. Optical Studies

3.4.1. Optical Transmission

The optical transmission studies were conducted on all the post-deposition annealed films using a UV-Visible spectrophotometer for the wavelength range of 200–800 nm. The deposition of thin films in this research work was conducted on quartz substrates. It is important to note that the results of XRD analysis and the structural changes in the films play a significant role in the transmission data of the films. From Figure 5, it can be seen that when the Cu_2O sputtering power is increased, the optical transmission shows a downward trend. The highest optical transmission was obtained for the films deposited with the lowest Cu_2O sputtering power of 10 W. This is possibly due to the films being Cr_2O_3 phase rich as indicated through XPS and XRD results. Additionally, Cr_2O_3 thin films have been previously reported to have a high optical transmission [57–61]. The lowest optical transmission was obtained for the films deposited with 100 W of Cu_2O sputtering power, possibly due to the films being CuO phase rich. The optical transmission of the films gets negatively affected due to the higher sputtering power of Cu_2O as the presence of the CuO

phase in the film has been previously reported to lower the overall optical transmission of the film [62–64]. The highest optical transmission of the single-phase CuCrO_2 thin films was identified to be ~81% at 700 nm wavelength obtained for film sputtered with 50 W of Cu_2O sputtering power.

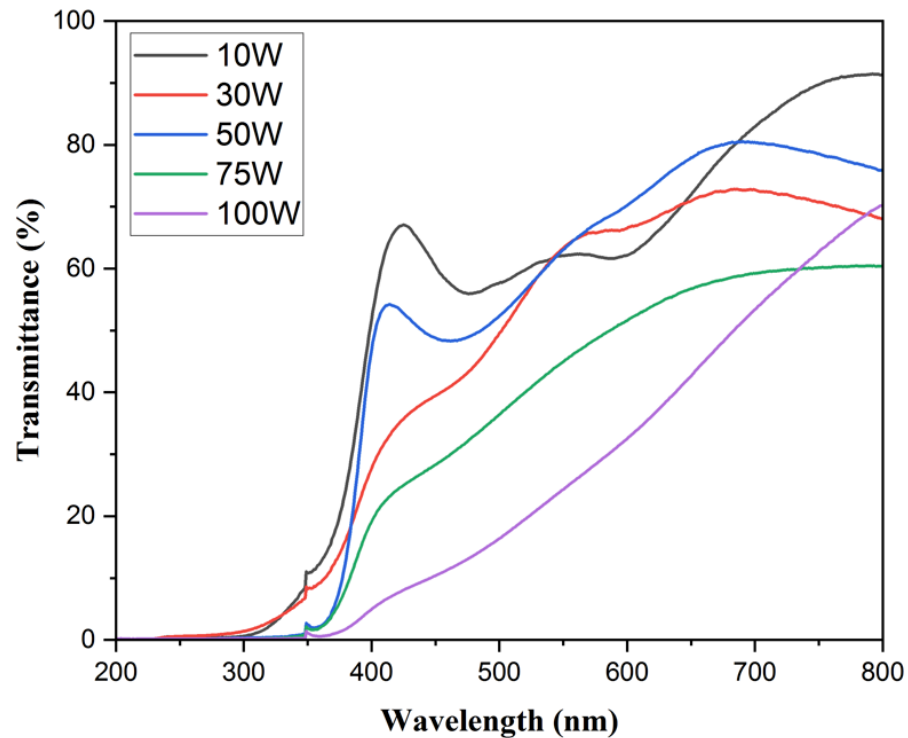


Figure 5. Optical transmission of the films deposited with varying Cu_2O sputtering powers.

3.4.2. Optical Bandgap

The optical transmission data were used to calculate the optical bandgap of the films deposited with varying Cu_2O sputtering powers using the Tauc plot method [65]. The absorption coefficient of the films was calculated using the relation,

$$\alpha = -\frac{2.303}{t} * \log_{10}(\%T) \quad (3)$$

where ‘ t ’ is the thickness and ‘ $\%T$ ’ is the optical transmission data obtained for the thin film. The band gap was calculated from the absorption coefficient using the Tauc equation,

$$(\alpha h\nu)^{\left(\frac{1}{n}\right)} = B(h\nu - E_g) \quad (4)$$

where $h\nu$ is the photon energy, and ‘ n ’ denotes the nature of sample transition. It has been reported previously that the value of n equals $1/2$, 2 , and $3/2$ for direct allowed, indirect allowed, and direct-forbidden transitions, respectively [65–67]. However, the films deposited in this research exhibit direct bandgap transition, since the best linear fit of the $(\alpha h\nu)^{\left(\frac{1}{n}\right)}$ versus the photon energy curve was obtained for $n = 1/2$. The Tauc plot thus obtained for the films sputtered at different Cu_2O sputtering powers is shown in Figure 6.

The optical bandgap of the films can be obtained from the Tauc plot by extending the linear portion of the curve to the x -axis. The optical bandgap of the films obtained for various Cu_2O sputtering powers is summarized in Table 5.

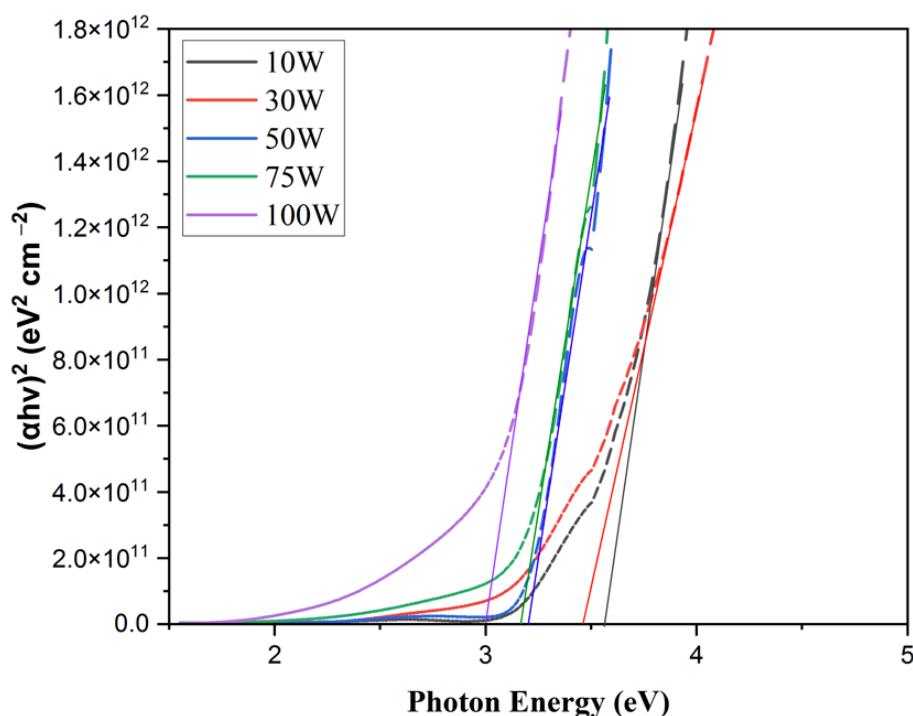


Figure 6. Tauc plot of the films deposited at various Cu_2O sputtering powers.

Table 5. Optical bandgap values of the films obtained at various Cu_2O sputtering powers.

Cu_2O Sputtering Powers (W)	Bandgap (eV)
10	3.62
30	3.46
50	3.21
75	3.16
100	3.00

It can be seen from Table 5 that with increasing Cu_2O sputtering powers, the optical bandgap of the films increases. The highest bandgap of 3.62 eV was obtained for the film deposited with 10W of Cu_2O sputtering power. With further increase in the sputtering power, the optical bandgap of the film decreased to a minimum value of 3.00 eV obtained for 100 W of Cu_2O sputtering power. This decrease in the optical bandgap can be attributed to the appearance of the CuO phase in the film. At lower sputtering powers of Cu_2O , the films are Cr_2O_3 phase rich. Due to this, the optical bandgap of the films obtained at lower Cu_2O sputtering powers was high. It has been previously reported that the optical bandgap of Cr_2O_3 thin films is close to the value of 3.62 eV obtained in this work [57–61]. As the Cu_2O sputtering power was increased, the films transitioned from being Cr_2O_3 phase rich to being CuO phase rich. CuO has a lower optical bandgap of 1.98–2.43 eV [68,69]. However, due to the presence of the CuCrO_2 phase in the film, the optical bandgap of the resultant film increased. The optical bandgap of single-phase CuCrO_2 thin films obtained in this work is 3.21 eV which correlated well with the values previously reported in the literature [33,41,70–74].

3.5. Electrical Studies

Electrical studies were performed on all the films in this research to study the variation of electrical resistivities of the films with the variation of Cu_2O sputtering power. The p-type conductivity of the films sputtered at Cu_2O sputtering power of 50 W and higher was verified with the help of the hot probe method and a four-point probe. This behavior can be attributed to the presence of the CuCrO_2 phase in the aforementioned films. The film

deposited with 10 W of Cu_2O sputtering power shows the highest resistivity of $27.64 \text{ K}\Omega\text{-cm}$. The reason for this high resistivity can be potentially due to the film being Cr_2O_3 phase rich. Cr_2O_3 , being a dielectric material, has been reported to show a very high electrical resistivity, to the order of several $\text{K}\Omega$ [58,75,76]. As the Cu_2O sputtering power increased to 30 W, the Cr_2O_3 content in the film dropped, which is evident from the peak intensity of XRD diffractograms. This resulted in $151.99 \text{ }\Omega\text{-cm}$ of electrical resistivity observed for 30 W of Cu_2O sputtering power. The lowest electrical resistivity of $0.652 \text{ }\Omega\text{-cm}$ was obtained for the film deposited with 50 W of Cu_2O sputtering power. The reason for the low resistivity in this film can be attributed to the identification of the single-phase delafossite nature of CuCrO_2 through XPS and XRD analysis. With the increase in Cu_2O sputtering power to 75 W and 100 W, the electrical resistivity starts to climb and reaches a value of $1.03 \text{ }\Omega\text{-cm}$ and $114.12 \text{ }\Omega\text{-cm}$. This is possibly due to the disintegration of the single-phase nature of CuCrO_2 film to a two-phase structure with the appearance of the CuO phase in the films along with the presence of the CuCrO_2 phase. CuO has been previously reported to display an increased resistivity to the order of $10^4 \text{ }\Omega\text{-cm}$ at a higher annealing temperature of $650 \text{ }^\circ\text{C}$ [1]. However, the resistivity obtained in this research work for the films sputtered with 75 W and 100 W of Cu_2O is comparatively lower due to the presence of the CuCrO_2 phase along with the CuO phase. Previously reported resistivity values for phase-pure CuCrO_2 thin films are close to $0.652 \text{ }\Omega\text{-cm}$ value obtained in this research [32,47,77]. A “V” shaped curve, as shown in Figure 7, was obtained when the trend of electrical resistivity was studied for variation in Cu_2O sputtering power.

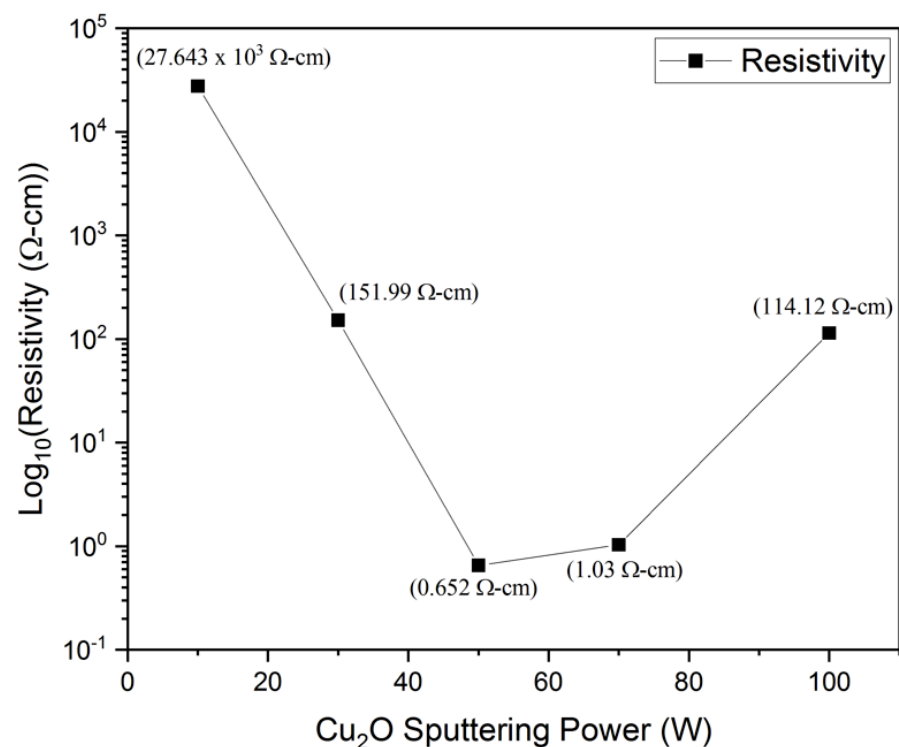


Figure 7. Variation of electrical resistivity with changes in Cu_2O sputtering powers.

4. Conclusions

In this research work, CuCrO_2 thin films were successfully synthesized using the RF magnetron sputtering technique of Cu_2O and Cr_2O_3 targets. The films thus obtained were post-deposition annealed at $650 \text{ }^\circ\text{C}$ in N_2 ambience. Through this work, it was found that the variation in the Cu_2O sputtering power played a key role in the electrical, optical, and structural properties of the films. XRD analysis confirmed that the single-phase delafossite nature of CuCrO_2 films is only obtained at 50 W of Cu_2O sputtering power. Sputtering at higher or lower powers resulted in the formation of films with a two-phase

structure. Distinctive differences between the core level spectrums of Cu-2p and Cr-2p were observed through XPS analysis as the Cu₂O sputtering power was varied. Cu LMM Auger peak was observed in the films identified with the CuCrO₂ phase. With the appearance of CuO and CuCr₂O₄ phases in the film, satellite peaks were observed in the Cu-2p core level spectra of the respective films. However, only films sputtered with 50 W of Cu₂O power showed Cu LMM Auger peak and no satellite peak presence in the Cu-2p core level spectrum. The formation of single-phase delafossite structure of CuCrO₂ was further confirmed from the results of EDS study that revealed a near stoichiometric ratio of 1:1.06 for Cu:Ga at% at 50 W of Cu₂O sputtering power. The optical studies revealed that the optical transmission and optical bandgap showed a downward trend as the Cu₂O sputtering power was increased. An optical transmission of ~ 81% at 700 nm wavelength and an optical bandgap of 3.21 eV were obtained for the single-phase CuCrO₂ thin film. The lowest resistivity value of 0.652 Ω-cm was obtained for the film deposited with 50 W of Cu₂O sputtering power. Hence, it can be concluded that 50 W of Cu₂O sputtering power was necessary for this research work to obtain the phase pure delafossite structure of CuCrO₂ thin film. The low electrical resistivity value obtained for single-phase CuCrO₂ thin film in this research work makes it an ideal candidate for use as an active material in transparent electronic devices such as thin-film diodes and transistors.

Author Contributions: Conceptualization, K.B.S.; Methodology, S.S. and K.B.S.; Validation, S.S.; Formal analysis, S.S.; Investigation, S.S. and A.H.B.; Data curation, S.S.; Writing—original draft, S.S.; Writing—review & editing, S.S. and K.B.S.; Visualization, S.S.; Supervision, K.B.S. All authors have read and agreed to the published version of the manuscript.

Funding: The APC was partially funded by The College of Graduate Studies, University of Central Florida, Orlando, FL 32826.

Institutional Review Board Statement: Not applicable.

Informed Consent Statement: Not applicable.

Data Availability Statement: Not applicable.

Acknowledgments: The authors would like to acknowledge the NSF MRI: ECCS: 1726636 and MCF-AMPAC facility, MSE, and CECS for the XPS use.

Conflicts of Interest: The authors declare no conflict of interest.

References

1. Hu, L.; Wei, R.H.; Tang, X.W.; Lu, W.J.; Zhu, X.B.; Sun, Y.P. Design strategy for p-type transparent conducting oxides. *J. Appl. Phys.* **2020**, *128*, 140902. [[CrossRef](#)]
2. Stadler, A. Transparent Conducting Oxides—An Up-to-Date Overview. *Materials* **2012**, *5*, 661–683. [[CrossRef](#)] [[PubMed](#)]
3. Afre, R.A.; Sharma, N.; Sharon, M.; Sharon, M. Transparent Conducting Oxide Films for Various Applications: A Review. *Rev. Adv. Mater. Sci.* **2018**, *53*, 79–89. [[CrossRef](#)]
4. Lan, J.-H.; Kanicki, J.; Catalano, A.; Keane, J.; Boer, W.D.; Gu, T. Patterning of transparent conducting oxide thin films by wet etching for a-Si:H TFT-LCDs. *J. Electron. Mater.* **1996**, *25*, 1806–1817. [[CrossRef](#)]
5. Sundaresh, S.; Nehate, S.D.; Sundaram, K.B. Electrical and Optical Studies of Reactively Sputtered Indium Oxide Thin Films. *ECS J. Solid State Sci. Technol.* **2021**, *10*, 065016. [[CrossRef](#)]
6. Bel Hadj Tahar, R.; Ban, T.; Ohya, Y.; Takahashi, Y. Optical, structural, and electrical properties of indium oxide thin films prepared by the sol-gel method. *J. Appl. Phys.* **1997**, *82*, 865–870. [[CrossRef](#)]
7. Bellingham, J.R.; Phillips, W.A.; Adkins, C.J. Electrical and optical properties of amorphous indium oxide. *J. Phys. Condens. Matter* **1990**, *2*, 6207. [[CrossRef](#)]
8. Xu, J.; Liu, J.-B.; Liu, B.-X.; Li, S.-N.; Wei, S.-H.; Huang, B. Design of n-Type Transparent Conducting Oxides: The Case of Transition Metal Doping in In₂O₃. *Adv. Electron. Mater.* **2018**, *4*, 1700553. [[CrossRef](#)]
9. Fallah, H.; Ghasemi, M.; Hassanzadeh, A.; Steki, H. The effect of annealing on structural, electrical and optical properties of nanostructured ITO films prepared by e-beam evaporation. *Mater. Res. Bull.* **2007**, *42*, 487–496. [[CrossRef](#)]
10. George, J.; Menon, C.S. Electrical and optical properties of electron beam evaporated ITO thin films. *Surf. Coat. Technol.* **2000**, *132*, 45–48. [[CrossRef](#)]
11. Dixon, S.C.; Sathasivam, S.; Williamson, B.A.D.; Scanlon, D.O.; Carmalt, C.J.; Parkin, I.P. Transparent conducting n-type ZnO:Sc—Synthesis, optoelectronic properties and theoretical insight. *J. Mater. Chem. C* **2017**, *5*, 7585–7597. [[CrossRef](#)]

12. Samadi, M.; Zirak, M.; Naseri, A.; Khorashadizade, E.; Moshfegh, A.Z. Recent progress on doped ZnO nanostructures for visible-light photocatalysis. *Thin Solid Films* **2016**, *605*, 2–19. [CrossRef]
13. Terrier, C.; Chatelon, J.P.; Roger, J.A. Electrical and optical properties of Sb:SnO₂ thin films obtained by the sol-gel method. *Thin Solid Films* **1997**, *295*, 95–100. [CrossRef]
14. Cheng, D.; Zhang, M.; Chen, J.; Yang, C.; Zeng, X.; Cao, D. Computer Screening of Dopants for the Development of New SnO₂-Based Transparent Conducting Oxides. *J. Phys. Chem. C* **2014**, *118*, 2037–2043. [CrossRef]
15. Shan, F.; Yu, Y. Band gap energy of pure and Al-doped ZnO thin films. *J. Eur. Ceram. Soc.* **2004**, *24*, 1869–1872. [CrossRef]
16. Maldonado, F.; Stashans, A. Al-doped ZnO: Electronic, electrical and structural properties. *J. Phys. Chem. Solids* **2010**, *71*, 784–787. [CrossRef]
17. Shantheyanda, B.P.; Todi, V.O.; Sundaram, K.B.; Vijayakumar, A.; Oladeji, I. Compositional study of vacuum annealed Al doped ZnO thin films obtained by RF magnetron sputtering. *J. Vac. Sci. Technol. A* **2011**, *29*, 051514. [CrossRef]
18. Mariappan, R.; Ponnuswamy, V.; Suresh, P.; Suresh, R.; Ragavendar, M.; Sankar, C. Deposition and characterization of pure and Cd doped SnO₂ thin films by the nebulizer spray pyrolysis (NSP) technique. *Mater. Sci. Semicond. Process.* **2013**, *16*, 825–832. [CrossRef]
19. de Moure-Flores, F.; Quiñones-Galván, J.G.; Hernández-Hernández, A.; Guillén-Cervantes, A.; Santana-Aranda, M.A.; Olvera, M.d.l.L.; Meléndez-Lira, M. Structural, optical and electrical properties of Cd-doped SnO₂ thin films grown by RF reactive magnetron co-sputtering. *Appl. Surf. Sci.* **2012**, *258*, 2459–2463. [CrossRef]
20. Saikumar, A.K.; Sundaresh, S.; Sundaram, K.B. Preparation and Characterization of p-Type Copper Gallium Oxide (CuGaO₂) Thin Films by Dual Sputtering Using Cu and Ga₂O₃ Targets. *ECS J. Solid State Sci. Technol.* **2022**, *11*, 065010. [CrossRef]
21. Saikumar, A.K.; Sundaresh, S.; Nehate, S.D.; Sundaram, K.B. Preparation and Characterization of Radio Frequency Sputtered Delafossite p-type Copper Gallium Oxide (p-CuGaO₂) Thin Films. *ECS J. Solid State Sci. Technol.* **2022**, *11*, 023005. [CrossRef]
22. Banerjee, A.; Chattopadhyay, K. Recent developments in the emerging field of crystalline p-type transparent conducting oxide thin films. *Prog. Cryst. Growth Charact. Mater.* **2005**, *50*, 52–105. [CrossRef]
23. Lamarsh, J.R.; Baratta, A.J. *Introduction to Nuclear Engineering*, 3rd ed.; Prentice Hall: Upper Saddle River, NJ, USA, 2017.
24. Ott, K.; Bezella, W.A. *Introductory Nuclear Reactor Statics Revised, Subsequent Edition*; Amer Nuclear Society: Indianapolis, IN, USA, 1989.
25. Zhang, K.H.L.; Xi, K.; Blamire, M.G.; Egdell, R.G. P-type transparent conducting oxides. *J. Phys. Condens. Matter* **2016**, *28*, 383002. [CrossRef] [PubMed]
26. Moreira, M.; Afonso, J.; Crepelliere, J.; Lenoble, D.; Lunca-Popa, P. A review on the p-type transparent Cu–Cr–O delafossite materials. *J. Mater. Sci.* **2022**, *57*, 3114–3142. [CrossRef]
27. Kawazoe, H.; Yasukawa, M.; Hyodo, H.; Kurita, M.; Yanagi, H.; Hosono, H. P-type electrical conduction in transparent thin films of CuAlO₂. *Nature* **1997**, *389*, 939–942. [CrossRef]
28. Nagarajan, R.; Duan, N.; Jayaraj, M.K.; Li, J.; Vanaja, K.A.; Yokochi, A.; Draeseke, A.; Tate, J.; Sleight, A.W. p-Type conductivity in the delafossite structure. *Int. J. Inorg. Mater.* **2001**, *3*, 265–270. [CrossRef]
29. Zhang, N.; Sun, J.; Gong, H. Transparent p-Type Semiconductors: Copper-Based Oxides and Oxychalcogenides. *Coatings* **2019**, *9*, 137. [CrossRef]
30. Scanlon, D.O.; Walsh, A. Polymorph engineering of CuMO₂ (M = Al, Ga, Sc, Y) semiconductors for solar energy applications: From delafossite to wurtzite. *Acta Crystallogr. Sect. B Struct. Sci.* **2015**, *71*, 702–706. [CrossRef]
31. Bai, Z.; Chen, S.-C.; Lin, S.-S.; Shi, Q.; Lu, Y.-B.; Song, S.-M.; Sun, H. Review in optoelectronic properties of p-type CuCrO₂ transparent conductive films. *Surf. Interfaces* **2021**, *22*, 100824. [CrossRef]
32. Chiba, H.; Hosaka, N.; Kawashima, T.; Washio, K. Thermal solid-phase crystallization of amorphous CuCrO₂:N thin films deposited by reactive radio-frequency magnetron sputtering. *Thin Solid Films* **2018**, *652*, 16–22. [CrossRef]
33. Obulapathi, L. Effect of Annealing Temperature on Structural, Electrical and Optical Properties of CuCrO₂ Thin Films by Reactive dc Magnetron Sputtering. *Indian J. Pure Appl. Physics.* 2014. Available online: <http://www.urpjournals.com:16-19> (accessed on 25 December 2022).
34. Yu, R.-S.; Tasi, C.-P. Structure, composition and properties of p-type CuCrO₂ thin films. *Ceram. Int.* **2014**, *40*, 8211–8217. [CrossRef]
35. Ahmadi, M.; Asemi, M.; Ghanaatshoar, M. Improving the electrical and optical properties of CuCrO₂ thin film deposited by reactive RF magnetron sputtering in controlled N₂/Ar atmosphere. *Appl. Phys. A* **2018**, *124*, 529. [CrossRef]
36. Chiu, T.-W.; Yang, Y.-C.; Yeh, A.-C.; Wang, Y.-P.; Feng, Y.-W. Antibacterial property of CuCrO₂ thin films prepared by RF magnetron sputtering deposition. *Vacuum* **2013**, *87*, 174–177. [CrossRef]
37. Yu, R.-S.; Hu, D.-H. Formation and characterization of p-type semiconductor CuCrO₂ thin films prepared by a sol-gel method. *Ceram. Int.* **2015**, *41*, 9383–9391. [CrossRef]
38. Yu, R.-S.; Wu, C.-M. Characteristics of p-type transparent conductive CuCrO₂ thin films. *Appl. Surf. Sci.* **2013**, *282*, 92–97. [CrossRef]
39. Ahmadi, M.; Asemi, M.; Ghanaatshoar, M. Mg and N co-doped CuCrO₂: A record breaking p-type TCO. *Appl. Phys. Lett.* **2018**, *113*, 242101. [CrossRef]
40. Novikov, V.; Xanthopoulou, G.; Knysh, Y.; Amosov, A. Solution Combustion Synthesis of nanoscale Cu–Cr–O spinels: Mechanism, properties and catalytic activity in CO oxidation. *Ceram. Int.* **2017**, *43*, 11733–11742. [CrossRef]

41. Bottiglieri, L. *Out of Stoichiometry CuCrO₂ as Transparent p-Type Semiconductor for Photovoltaics and Transparent Electronics CuCrO₂ Hors Stoechiométrie Comme Semi-Conducteur Transparent de Type p Pour le Photovoltaïque et l'électronique Transparente*; Université Grenoble Alpes: Grenoble, France, 2022.
42. Bottiglieri, L.; Resende, J.; Weber, M.; Chaix-Pluchery, O.; Jiménez, C.; Deschamps, J.-L. Out of stoichiometry CuCrO₂ films as a promising p-type TCO for transparent electronics. *Mater. Adv.* **2021**, *2*, 4721–4732. [[CrossRef](#)]
43. Chen, H.-Y.; Chang, K.-P. Influence of Post-Annealing Conditions on the Formation of Delafossite-CuCrO₂ Films. *ECS J. Solid State Sci. Technol.* **2013**, *2*, P76. [[CrossRef](#)]
44. Sundaresh, S.; Saikumar, A.K.; Sundaram, K.B. Investigation on the Intermixing of Cu and in Layers for the Formation of Cu₂In₂O₅ Thin Films. *ECS J. Solid State Sci. Technol.* **2022**, *11*, 085003. [[CrossRef](#)]
45. Chen, H.-Y.; Yang, W.-J.; Chang, K.-P. Characterization of delafossite-CuCrO₂ thin films prepared by post-annealing using an atmospheric pressure plasma torch. *Appl. Surf. Sci.* **2012**, *258*, 8775–8779. [[CrossRef](#)]
46. Crépellière, J.; Popa, P.L.; Bahlawane, N.; Leturcq, R.; Werner, F.; Siebentritt, S.; Lenoble, D. Transparent conductive CuCrO₂ thin films deposited by pulsed injection metal organic chemical vapor deposition: Up-scalable process technology for an improved transparency/conductivity trade-off. *J. Mater. Chem. C* **2016**, *4*, 4278–4287. [[CrossRef](#)]
47. Wu, S.; Deng, Z.; Dong, W.; Shao, J.; Fang, X. Effect of deposition atmosphere on the structure and properties of Mg doped CuCrO₂ thin films prepared by direct current magnetron sputtering. *Thin Solid Films* **2015**, *595*, 124–128. [[CrossRef](#)]
48. Le, T.; Flahaut, D.; Martinez, H.; Andreu, N.; Gonbeau, D.; Pachoud, E.; Pelloquin, D.; Maignan, A. The electronic structure of the CuRh_{1-x}Mg_xO₂ thermoelectric materials: An X-ray photoelectron spectroscopy study. *J. Solid State Chem.* **2011**, *184*, 2387–2392. [[CrossRef](#)]
49. Vankudoth, K.; Gutta, N.; Velisoju, V.K.; Mutyala, S.; Aytam, H.P.; Akula, V. CuCr₂O₄ derived by the sol-gel method as a highly active and selective catalyst for the conversion of glycerol to 2,6-dimethylpyrazine: A benign and eco-friendly process. *Catal. Sci. Technol.* **2017**, *7*, 3399–3407. [[CrossRef](#)]
50. Xiao, Z.; Xiu, J.; Wang, X.; Zhang, B.; Williams, C.T.; Su, D.; Liang, C. Controlled preparation and characterization of supported CuCr₂O₄ catalysts for hydrogenolysis of highly concentrated glycerol. *Catal. Sci. Technol.* **2013**, *3*, 1108–1115. [[CrossRef](#)]
51. Yang, B.; Ouyang, D.; Huang, Z.; Ren, X.; Zhang, H.; Choy, W.C.H. Multifunctional Synthesis Approach of In:CuCrO₂ Nanoparticles for Hole Transport Layer in High-Performance Perovskite Solar Cells. *Adv. Funct. Mater.* **2019**, *29*, 1902600. [[CrossRef](#)]
52. Yu, R.-S.; Chu, C. Synthesis and Characteristics of Zn-Doped CuCrO₂ Transparent Conductive Thin Films. *Coatings* **2019**, *9*, 321. [[CrossRef](#)]
53. Biesinger, M.C.; Brown, C.; Mycroft, J.R.; Davidson, R.D.; McIntyre, N.S. X-ray photoelectron spectroscopy studies of chromium compounds. *Surf. Interface Anal.* **2004**, *36*, 1550–1563. [[CrossRef](#)]
54. Biesinger, M.C.; Payne, B.P.; Grosvenor, A.P.; Lau, L.W.M.; Gerson, A.R.; Smart, R.S.C. Resolving surface chemical states in XPS analysis of first row transition metals, oxides and hydroxides: Cr, Mn, Fe, Co and Ni. *Appl. Surf. Sci.* **2011**, *257*, 2717–2730. [[CrossRef](#)]
55. Lin, F.; Gao, C.; Zhou, X.; Shi, W.; Liu, A. Magnetic, electrical and optical properties of p-type Fe-doped CuCrO₂ semiconductor thin films. *J. Alloys Compd.* **2013**, *581*, 502–507. [[CrossRef](#)]
56. Deng, L.; Lin, F.; Yu, Q.; He, X.; Liu, A.; Shi, W.; Feng, J. Improved ferromagnetic behavior and novel near-infrared photoluminescence in Mg/Mn-codoped CuCrO₂ ceramics. *J. Mater. Sci.* **2016**, *51*, 7491–7501. [[CrossRef](#)]
57. Al-Kuhaili, M.; Durrani, S. Optical properties of chromium oxide thin films deposited by electron-beam evaporation. *Opt. Mater.* **2007**, *29*, 709–713. [[CrossRef](#)]
58. Singh, J.; Verma, V.; Kumar, R.; Kumar, R. Structural, optical and electrical characterization of epitaxial Cr₂O₃ thin film deposited by PLD. *Mater. Res. Express* **2019**, *6*, 106406. [[CrossRef](#)]
59. Julkarnain, M.; Hossain, J.; Khan, K. Temperature effect on the electrical properties of chromium oxide (Cr₂O₃) thin films. *J. Optoelectron. Adv. Mater.* **2011**, *13*, 485–490.
60. Ivanova, T.; Surtchev, M.; Gesheva, K. Characterization of CVD Chromium Oxide Thin Films. *Phys. Status Solidi (A)* **2001**, *184*, 507–513. [[CrossRef](#)]
61. Julkarnain, M.; Hossain, J.; Khan, K. Optical properties of thermally evaporated Cr₂O₃ thin films. *Can. J. Chem. Eng. Technol.* **2012**, *3*, 81–85.
62. Baturay, S.; Tombak, A.; Kaya, D.; Oca, Y.S.; Tokus, M.; Aydemir, M.; Kilicoglu, T. Modification of electrical and optical properties of CuO thin films by Ni doping. *J. Sol-Gel Sci. Technol.* **2016**, *78*, 422–429. [[CrossRef](#)]
63. Chen, A.; Yang, G.; Long, H.; Li, F.; Li, Y.; Lu, P. Nonlinear optical properties of laser deposited CuO thin films. *Thin Solid Films* **2009**, *517*, 4277–4280. [[CrossRef](#)]
64. Diachenko, O.; Kováč, J.; Dobrozhan, O.; Novák, P.; Kováč, J.; Skrinariova, J.; Opanasyuk, A. Structural and Optical Properties of CuO Thin Films Synthesized Using Spray Pyrolysis Method. *Coatings* **2021**, *11*, 1392. [[CrossRef](#)]
65. Tauc, J.; Grigorovici, R.; Vancu, A. Optical Properties and Electronic Structure of Amorphous Germanium. *Phys. Status Solidi B* **1966**, *15*, 627–637. [[CrossRef](#)]
66. Abeles, F. (Ed.) *Optical Properties of Solids*; North-Holland Pub. Co.: Amsterdam, The Netherlands; American Elsevier: New York, NY, USA, 1972.

67. Davis, E.A.; Mott, N.F. Conduction in non-crystalline systems V. Conductivity, optical absorption and photoconductivity in amorphous semiconductors. *Philos. Mag.* **1970**, *22*, 0903–0922. [[CrossRef](#)]
68. Dahrul, M.; Alatas, H. Irzaman Preparation and Optical Properties Study of CuO thin Film as Applied Solar Cell on LAPAN-IPB Satellite. *Procedia Environ. Sci.* **2016**, *33*, 661–667. [[CrossRef](#)]
69. Wang, H.; Xu, J.-Z.; Zhu, J.-J.; Chen, H.-Y. Preparation of CuO nanoparticles by microwave irradiation. *J. Cryst. Growth* **2002**, *244*, 88–94. [[CrossRef](#)]
70. Sánchez-Alarcón, R.L.; Oropeza-Rosario, G.; Gutierrez-Villalobos, A.; Muro-López, M.A.; Martínez-Martínez, R.; Zaleta-Alejandre, E.; Falcony, C.; Alarcón-Flores, G.; Fragoso, R.; Hernández-Silva, O.; et al. Ultrasonic spray-pyrolyzed CuCrO₂ thin films. *J. Phys. D Appl. Phys.* **2016**, *49*, 175102. [[CrossRef](#)]
71. Moreno-Camacho, C.A.; Montoya-Torres, J.R.; Jaegler, A.; Gondran, N. Sustainability metrics for real case applications of the supply chain network design problem: A systematic literature review. *J. Clean. Prod.* **2019**, *231*, 600–618. [[CrossRef](#)]
72. Zhou, X.; Lin, F.; Shi, W.; Liu, A. Structural, electrical, optical and magnetic properties of p-type Cu(Cr_{1-x}Mnx)O₂ thin films prepared by pulsed laser deposition. *J. Alloy. Compd.* **2014**, *614*, 221–225. [[CrossRef](#)]
73. Chen, H.-Y.; Chang, K.-P.; Yang, C.-C. Characterization of transparent conductive delafossite-CuCr_{1-x}O₂ films. *Appl. Surf. Sci.* **2013**, *273*, 324–329. [[CrossRef](#)]
74. Shin, D.; Foord, J.S.; Egdell, R.G.; Walsh, A. Electronic structure of CuCrO₂ thin films grown on Al₂O₃(001) by oxygen plasma assisted molecular beam epitaxy. *J. Appl. Phys.* **2012**, *112*, 113718. [[CrossRef](#)]
75. Mahmood, A.; Street, M.; Echtenkamp, W.; Kwan, C.P.; Bird, J.P.; Binek, C. Dielectric properties of thin Cr₂O₃ films grown on elemental and oxide metallic substrates. *Phys. Rev. Mater.* **2018**, *2*, 044401. [[CrossRef](#)]
76. De Los Santos Valladares, L.; Salinas, D.H.; Dominguez, A.B.; Najarro, D.A.; Khondaker, S.I.; Mitrelias, T.; Barnes, C.H.W.; Aguiar, J.A.; Majima, Y. Crystallization and electrical resistivity of Cu₂O and CuO obtained by thermal oxidation of Cu thin films on SiO₂/Si substrates. *Thin Solid Films* **2012**, *520*, 6368–6374. [[CrossRef](#)]
77. Jantrasee, S.; Ruttanapun, C. Impact of Sn⁴⁺ Substitution at Cr³⁺ Sites on Thermoelectric and Electronic Properties of p-Type Delafossite CuCrO₂. *J. Electron. Mater.* **2019**, *49*, 601–610. [[CrossRef](#)]

Disclaimer/Publisher's Note: The statements, opinions and data contained in all publications are solely those of the individual author(s) and contributor(s) and not of MDPI and/or the editor(s). MDPI and/or the editor(s) disclaim responsibility for any injury to people or property resulting from any ideas, methods, instructions or products referred to in the content.